Journal of Materials Chemistry

Cite this: J. Mater. Chem., 2012, 22, 9826

www.rsc.org/materials

PAPER

Thermoelectric properties of Zn-doped Ca_3AlSb_3

Wolfgang G. Zeier,†[ab] Alex Zevalkink,†[a] Eugen Schechtel,[a] Wolfgang Tremel[b] and G. Jeffrey Snyder*[a]

Received 3rd March 2012, Accepted 23rd March 2012
DOI: 10.1039/c2jm31324c

Polycrystalline samples of $Ca_3Al_{1-x}Zn_xSb_3$, with $x = 0.00$, 0.01, 0.02, and 0.05 were synthesized *via* a combined ball milling and hot pressing technique and the influence of zinc as a dopant on the thermoelectric properties was studied and compared to the previously reported transport properties of sodium-doped Ca_3AlSb_3. Consistent with the transport in the sodium-doped material, substitution of aluminum with zinc leads to p-type carrier conduction that can be sufficiently explained with a single parabolic band model. It is found that, while exhibiting higher carrier mobilities, the doping effectiveness of zinc is lower than that of sodium and the optimum carrier concentration for a maximum figure of merit zT is not reached in this study. We find that the grain size influences the carrier mobility, carrier concentration, and lattice thermal conductivity, leading to improved properties at intermediate temperatures, and highlighting a possible approach for improved figures of merit in this class of materials.

1 Introduction

In the ongoing search for new materials for thermoelectric applications such as waste heat recovery and power generation, materials composed of inexpensive and earth abundant elements need to be explored and their thermoelectric efficiencies improved. The thermoelectric efficiency is determined by the figure of merit $zT = \alpha^2 T/\rho\kappa$. Thus, an ideal thermoelectric material requires a large Seebeck coefficient α, low electrical resistivity ρ, and low thermal conductivity κ.[1]

Zintl compounds, such as $Yb_{14}MnSb_{11}$, $Ca_5Al_2Sb_6$, AZn_2Sb_2 (*e.g.* A = Ca, Yb, Eu), $Ba_8Ga_{16}Ge_{30}$ and $CsBi_4Te_6$,[2–10] have been shown to be promising candidates for thermoelectric materials due to their complex crystal structures, resulting in low lattice thermal conductivities, and the possibility of precise doping to optimize the Seebeck coefficient and electrical resistivity.[11–13]

In the family of Zintl antimonides, Ca_3AlSb_3 is another interesting compound with a peak zT of 0.8 obtained at 1050 K upon doping with Na^+ for Ca^{2+}.[14] Our previous investigation of Ca_3AlSb_3 shows an intrinsic semiconductor with a band gap of 0.6 eV and very low lattice thermal conductivity (0.6 W/mK at 870 K) due to a relatively complex crystal structure. While doping with sodium leads to the formation of holes and degenerate transport behavior, a low solubility limit leads to a maximum of 4×10^{19} holes/cm^3, whereas the optimum carrier density for a maximum zT is expected to be greater than 5×10^{19} holes/cm^3.[14]

Inspired by our previous investigation of Ca_3AlSb_3 and the doping studies with sodium and zinc in $Ca_5Al_2Sb_6$,[4,5,14] here we explore the influence of the substitution of Al with Zn on the thermoelectric transport properties of the $Ca_3Al_{1-x}Zn_xSb_3$ system, and compare the effects of Na- and Zn-doping on hole carrier concentrations, mobilities of the charge carriers, and the thermoelectric figure of merit. Furthermore we report on the influence of the grain size in these materials on the thermoelectric transport.

2 Experimental

Bulk, polycrystalline $Ca_3Al_{1-x}Zn_xSb_3$ samples with compositions $x = 0.00$, 0.01, 0.02, and 0.05 were prepared by ball milling followed by hot pressing from elemental Ca (Sigma-Aldrich, 99.9%, dendritic pieces), Al (Alfa Aesar, 99.9%, shot), Zn (Alfa Aesar, 99.99%, shot) and Sb (Alfa Aesar, 99.9999%, shot). The elements were slivered into small pieces and loaded into stainless-steel vials with stainless-steel balls in an Ar dry box. The precursors were milled for 90 min using a SPEX Sample Prep 8000 Series Mixer/Mill. The resulting powder was consolidated by induction hot pressing in high density graphite dies.[15] The die was slowly heated up to 973 K in two hours then held at this temperature at a pressure of 40 MPa for four hours, and five hours for $x = 0.01$, respectively. After a stress free two hour cool down, the resulting ingots were sliced into 1–1.5 mm thick disks, 12 mm in diameter, and characterized.

X-ray diffraction measurements were performed on a Philips PANalytical X'Pert Pro with Cu-Kα radiation and a step size of 0.0084°. Pawley refinements were performed with TOPAS

[a]*Materials Science, California Institute of Technology, 1200 E. California Blvd., Pasadena, CA 91125, USA. E-mail: jsnyder@caltech.edu; Fax: +1 (626) 395-8868; Tel: +1 (626) 395-6220*
[b]*Institut für Anorganische Chemie und Analytische Chemie der Johannes Gutenberg-Universität, Duesbergweg 10-14, D-55099 Mainz, Germany*
† These authors contributed equally to this work.

Academic V4.1[16] applying the fundamental parameter approach using the crystallographic data from Cordier *et al.*[17] Scanning electron microscopy (SEM) images and energy-dispersive X-ray spectroscopy (EDS) of the consolidated materials were taken using a Zeiss 1550 VP SEM. Thermal diffusivity was measured using a Netzsch laser flash diffusivity instrument (LFA 457) with samples coated in a thin layer of graphite to minimize errors in the emissivity. The data were analyzed using a Cowan model with pulse correction. Heat capacity (C_p) was estimated using the method of Dulong-Petit ($C_p = 3R$, k_B per atom), which is likely to result in an underestimation (~10%) of the thermal conductivity at high temperatures.[18]

The Seebeck coefficient was calculated from the slope of the thermopower *vs.* temperature gradient measurements from chromel-Nb thermocouples.[19] Electrical resistivity and Hall coefficients were measured using the Van der Pauw technique under a reversible magnetic field of 1T and pressure-assisted contacts. All measurements were performed under dynamic vacuum and the combined uncertainty for all measurements involved in zT determination is ~20%.

Electronic transport measurements were analyzed using common solutions to the Boltzmann transport equations within the relaxation time approximation under the assumption of a single parabolic band, as described for this compound in ref. 14.

3 Results and discussion

Following ball milling and hot pressing, $Ca_3Al_{1-x}Zn_xSb_3$ samples with $x = 0.00$, 0.01, 0.02, and 0.05 have geometric densities of at least 97% of the theoretical densities. As reported in ref. 14, X-ray diffraction (Fig. 1) and scanning electron microscopy reveal secondary phases of $Ca_5Al_2Sb_6$ and $Ca_{14}AlSb_{11}$ with 5–10wt% and 2–5wt%, respectively. SEM analysis of fracture surfaces reveals small grains (<1 μm in diameter) and porosity (0.1 μm in diameter) at the grain boundaries. However, the sample with the nominal composition of $Ca_3Al_{0.99}Zn_{0.01}Sb_3$ contains grains that are at least an order of magnitude larger, as shown in the inset of Fig. 3. The relatively small grains found in all samples in this study are in accordance with the broad profiles of the reflections in Fig. 1 and therefore no significant change of the lattice parameters upon substitution with Zn can be observed.

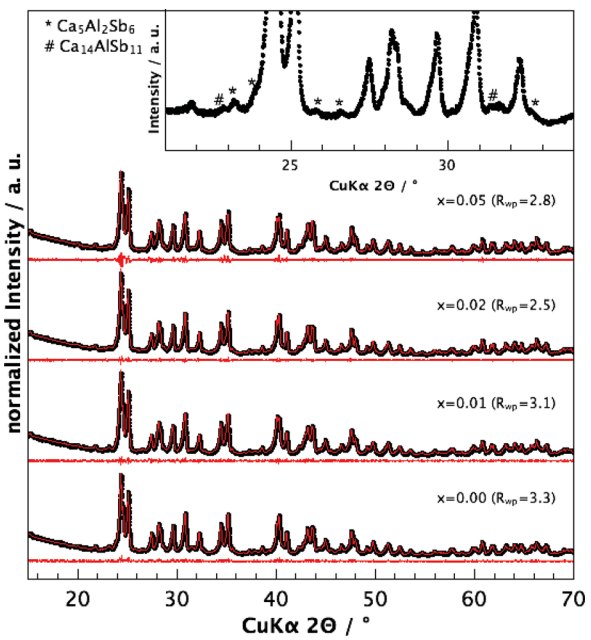

Fig. 1 X-ray diffraction data for $Ca_3Al_{1-x}Zn_xSb_3$ including profile fit, profile difference, and profile residuals from the corresponding Pawley refinement including the secondary phases of $Ca_5Al_2Sb_6$ and $Ca_{14}AlSb_{11}$. The inset shows the reflections indexed to the impurity phases, observed in all samples.

3.1 Electronic transport properties

The electronic properties of sodium doped Ca_3AlSb_3 have previously been investigated and are largely similar to those reported here with zinc as a dopant. In the following results we have included the transport properties of the Na-doped sample that resulted in the highest figure of merit (nominal composition $Ca_{2.94}Na_{0.06}AlSb_3$) as a basis for comparison.[14]

Fig. 2 shows the measured Hall carrier concentrations as a function of temperature. Though Ca_3AlSb_3 is a classic, valence-precise Zintl compound, the undoped material has a p-type carrier concentration of 10^{18} holes/cm^3 at room temperature due to intrinsic defects. As expected, the carrier concentration increases upon substitution of Al^{3+} with Zn^{2+} due to the introduction of holes. Doped samples behave extrinsically, with temperature independent carrier concentrations up to 700 K, after which the carrier concentration increases abruptly, likely due to carrier excitation across the band gap ($E_g \sim 0.6$ eV[14]). Zinc doping introduces significantly fewer holes than predicted, in accordance with our previous attempts at doping Ca_3AlSb_3 and the closely related phase, $Ca_5Al_2Sb_6$.[4,5,14] Ultimately, the maximum carrier concentration achieved by doping with zinc is lower than that achieved upon sodium doping, suggesting a lower solubility limit for zinc, assuming substitution of Al with Zn.

Impurities at grain boundaries, such as oxidation or possibly phases that are too small to observe by SEM, are already known to impede charge transport in Ca_3AlSb_3, leading to reduced mobility at low temperatures.[14] Grain boundaries are also a likely place for Zn to accumulate, potentially causing the reduced doping effectiveness observed in this study. This supposition is supported by the anomalous carrier concentration of the $x = 0.01$ sample, which is higher than that of the samples with $x = 0.02$ and 0.05, and may be attributable to its large grain size and thus lower interfacial surface area.

Grain size also correlates with the carrier mobility of the $Ca_3Al_{1-x}Zn_xSb_3$ samples in this study. The Hall mobility, calculated from the measured Hall coefficient (R_H) and resistivity (ρ), is shown in Fig. 2. For samples with sub-micron grains ($x = 0.0$, $x = 0.02$, and $x = 0.05$), the Hall mobility at low temperatures exhibits an exponential temperature dependence ($\mu_H = \mu_0 e^{-E_A/k_BT}$) indicative of a barrier at the grain boundaries, such as an oxide layer, requiring an activation energy to overcome. At higher temperatures (>600 K) the mobility is limited by acoustic phonon scattering, for which the temperature dependence is given by $\mu_H \propto T^{-\nu}$, with ν between 1 and 1.5 for

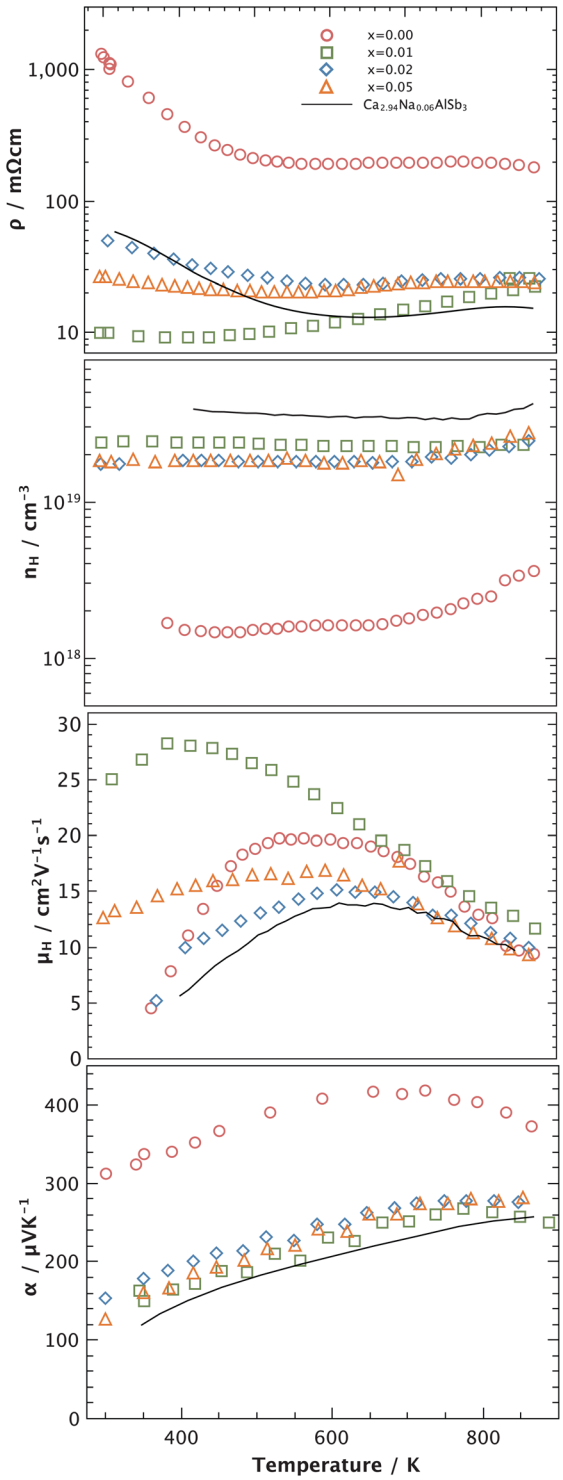

Fig. 2 Temperature dependence of the electrical resistivity ρ, the Hall carrier concentration n_H, the Hall mobility μ_H, and the Seebeck coefficient α of $Ca_3Al_{1-x}Zn_xSb_3$. Experimental data is compared to $Ca_{2.94}Na_{0.06}AlSb_3$ data (black line).[14]

degenerate and non-degenerate behavior, respectively.[20] However, the sample with the nominal composition of $Ca_3Al_{0.99}Zn_{0.01}Sb_3$ exhibits larger Hall mobilities than all other compositions, with acoustic phonon scattering dominating transport above 400 K. This suggests that since larger grains (inset of Fig. 3) result in a lower interfacial surface area, a less pronounced activation process in the temperature dependence of the Hall mobility in this sample leads to higher mobility at lower temperatures. Additionally, larger grain sizes may cause a larger carrier mobility at lower temperatures in the sample with $x = 0.01$ through reduced grain boundary scattering.

The temperature dependence of the electrical resistivity (Fig. 2) shows a decreasing trend at lower temperatures, consistent with the activated mobility behavior ($\rho = 1/ne\mu$). At higher temperatures the resistivity behaves as expected for a heavily doped semiconductor.

The Seebeck coefficients are positive, consistent with the p-type carrier concentrations, and the temperature dependence is shown in Fig. 2. The Seebeck coefficient of undoped Ca_3AlSb_3 increases up to a temperature of 700 K, at which point thermally activated electrons reduce the thermoelectric voltage resulting in a decay of the Seebeck coefficient. As expected for a heavily doped semiconductor, the Seebeck coefficients decrease with increasing carrier concentrations. In order to compare the influence of Zn and Na as dopants on the electronic structure of this material, the Pisarenko relation of this material is shown in Fig. 4. The experimental Seebeck and carrier concentrations were measured at 700 K, while the dashed line was generated using the single parabolic band model described in ref. 14 with a valence band effective mass of $m^* = 0.8m_e$. Both Zn and Na doped materials are well described by the same model, suggesting that

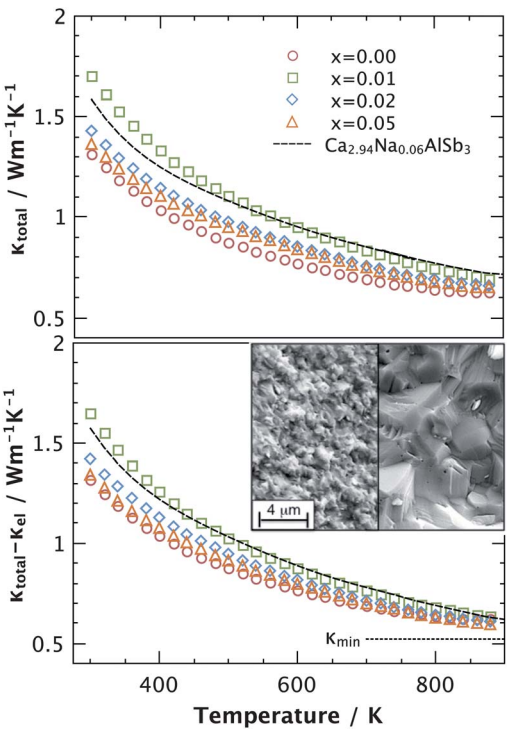

Fig. 3 Total thermal conductivity (top) and lattice thermal conductivity (bottom) of $Ca_3Al_{1-x}Zn_xSb_3$ with temperature, with the theoretical minimum lattice thermal conductivity at higher temperatures. The inset illustrates the different grain sizes of the samples. Smaller grains (left) for the compositions with $x = 0.00$, 0.02, and 0.05 and larger grain sizes for $x = 0.01$ (right).

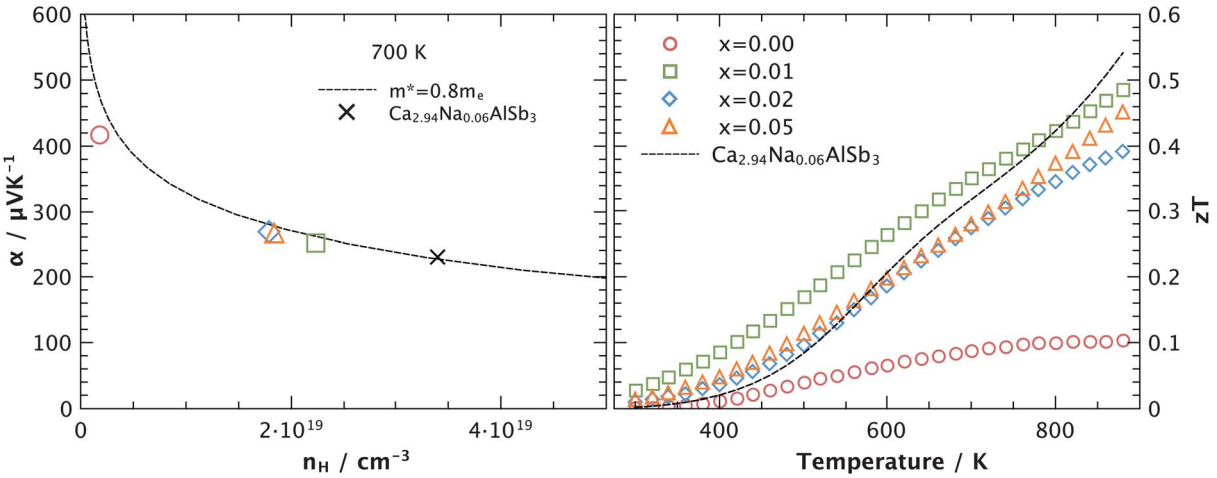

Fig. 4 Experimental Seebeck coefficients as a function of carrier concentration (left) and figure of merit zT with temperature of $Ca_3Al_{1-x}Zn_xSb_3$.

using Zn as a dopant does not affect the band structure of the compound.

3.2 Thermal transport properties

The total thermal conductivities, shown in Fig. 3, were calculated using $\kappa = DdC_p$ where D = thermal diffusivity, d = geometric density, C_p = specific heat capacity. The electronic contribution, κ_{el}, to the total thermal conductivity can be estimated from the Wiedemann-Franz relation ($\kappa_{el} = LT/\rho$). In this study, the Lorenz numbers L are calculated from the experimental Seebeck coefficients as described for this material in ref. 8 and 14. Subtracting the electronic term from the total thermal conductivity leaves the lattice thermal conductivity and the bipolar contribution. No significant bipolar contribution can be observed in this temperature range, which would be visible as an upturn in the data at higher temperatures, and therefore the resulting term is hereafter referred to as lattice thermal conductivity.

The lattice thermal conductivity is well described by a T^{-1}-dependence, characteristic of phonon-phonon Umklapp scattering.[21] The influence of Zn on the lattice thermal conductivity seems to be negligible, as reported in the sodium doped Ca_3AlSb_3. However, the sample with nominal composition $Ca_3Al_{0.99}Zn_{0.01}Sb_3$ exhibits a higher thermal conductivity at lower temperatures. This can be attributed to the larger grains in this sample. In contrast, the sub-micron grains in the other samples result in more boundary scattering, and thus reduced lattice thermal conductivities at lower temperatures. In all samples, the lattice thermal conductivities approach the minimum thermal conductivity κ_{min}, which was calculated using speed of sound measurements and Cahill's formula for disordered crystals.[14,22,23]

3.3 Figure of merit

The figure of merit of $Ca_3Al_{1-x}Zn_xSb_3$ is shown in Fig. 4. Doping with zinc increases the figure of merit, leading to a zT of 0.5 at 900 K for $x = 0.01$. Compared with the Na-doped samples of our previous investigation, all of the Zn-doped samples exhibit enhanced zT at intermediate temperatures, which can be attributed to their higher carrier mobilities. The $x = 0.01$ sample, which has the largest grain size and thus the highest mobility, shows the largest degree of zT enhancement. However, the peak zT values of the sodium doped Ca_3AlSb_3 samples can not be achieved with zinc due to its limited doping effectiveness when compared to Na.

4 Conclusion

The thermoelectric properties of zinc-doped Ca_3AlSb_3 were compared to a previously reported study on sodium as a dopant. A similar band mass and lattice thermal conductivity is observed regardless of whether Zn or Na is the dopant. However, zinc exhibits a lower solubility limit than sodium, resulting in lower carrier concentrations and a lower peak figure of merit, because the optimum carrier concentration for this material cannot be reached *via* doping with zinc. This study also shows the effect of different grain sizes on the thermoelectric transport properties, with larger grains leading to higher thermal conductivities and higher mobilities at lower temperatures, due to reduced scattering of phonons and electrons at the grain boundaries. Ultimately, we find that while larger grain size has little effect on the high temperature properties, the reduction of grain boundary surface area improves the figure of merit at intermediate temperatures. This work shows the common strategy to use nano-structured materials does not always lead to an improved figure of merit. Other competing factors such as a reduction in mobility may overwhelm the improvement of the lattice thermal conductivity.

Acknowledgements

We gratefully acknowledge the NASA Jet Propulsion Laboratory for support. Wolfgang Zeier thanks the Carl-Zeiss foundation and the Graduate School of Excellence MAINZ, funded by the State of Rhineland-Palatinate.

References

1 L. E. Bell, *Science*, 2008, **321**, 1457–1461.
2 E. S. Toberer, C. A. Cox, S. R. Brown, T. Ikeda, A. F. May, S. M. Kauzlarich and G. J. Snyder, *Adv. Funct. Mater.*, 2008, **18**, 2795–2800.

3 E. S. Toberer, S. R. Brown, T. Ikeda, S. M. Kauzlarich and G. J. Snyder, *Appl. Phys. Lett.*, 2008, **93**, 062110.
4 E. S. Toberer, A. Zevalkink, N. Crisosto and G. J. Snyder, *Adv. Funct. Mater.*, 2010, **20**, 4375–4380.
5 A. Zevalkink, E. S. Toberer, T. Bleith, E. Flage-Larsen and G. J. Snyder, *J. Appl. Phys.*, 2011, **110**, 013721.
6 F. Gascoin, S. Ottensmann, D. Stark, S. M. Haile and G. J. Snyder, *Adv. Funct. Mater.*, 2005, **15**, 1860–1864.
7 C. Yu, T. J. Zhu, S. N. Zhang, X. B. Zhao, J. He, Z. Su and T. M. Tritt, *J. Appl. Phys.*, 2008, **104**, 013705.
8 A. F. May, E. S. Toberer, A. Saramat and G. J. Snyder, *Phys. Rev. B: Condens. Matter Mater. Phys.*, 2009, **80**, 125205.
9 E. S. Toberer, M. Christensen, B. Iversen and G. Snyder, *Phys. Rev. B: Condens. Matter Mater. Phys.*, 2008, **77**, 1–8.
10 D. Chung, T. Hogan, P. Brazis, M. Rocci-Lane, C. Kannewurf, M. Bastea, C. Uher and M. G. Kanatzidis, *Science*, 2000, **287**, 1024–1027.
11 G. J. Snyder and E. S. Toberer, *Nat. Mater.*, 2008, **7**, 105–114.
12 E. S. Toberer, A. F. May and G. J. Snyder, *Chem. Mater.*, 2010, **22**, 624–634.
13 S. M. Kauzlarich, S. R. Brown and G. J. Snyder, *Dalton Trans.*, 2007, 2099–2107.
14 A. Zevalkink, E. S. Toberer, W. G. Zeier, E. Flage-Larsen and G. J. Snyder, *Energy Environ. Sci.*, 2011, **4**, 510.
15 A. D. LaLonde, T. Ikeda and G. J. Snyder, *Rev. Sci. Instrum.*, 2011, **82**, 025104.
16 A. Cohelo, *TOPAS Academic V4.1*, 2004.
17 G. Cordier, H. Schäfer and M. Stelter, *Z. Naturforsch.*, 1984, **39b**, 727–732.
18 O. Delaire, A. F. May, M. A. McGuire, W. D. Porter, M. S. Lucas, M. B. Stone, D. L. Abernathy, V. A. Ravi, S. A. Firdosy and G. J. Snyder, *Phys. Rev. B: Condens. Matter Mater. Phys.*, 2009, **80**, 184302.
19 S. Iwanaga, E. S. Toberer, A. LaLonde and G. J. Snyder, *Rev. Sci. Instrum.*, 2011, **82**, 063905.
20 Y. I. Ravich, B. A. Efimova and I. A. Smirnov, *Semiconducting Lead Chalcogenides*, Plenum Press, New York, 1970.
21 J. Yang, *Thermal Conductivity-Theory, Properties and Applications*, Kluwer Academic/Plenum Publishers, New York, 2004.
22 D. Cahill, S. Watson and R. Pohl, *Phys. Rev. B: Condens. Matter*, 1992, **46**, 6131–6140.
23 E. S. Toberer, A. Zevalkink and G. J. Snyder, *J. Mater. Chem.*, 2011, **21**, 15843–15852.